Eur. Phys. J. D (2018) 72: 66
https://doi.org/10.1140/epjd/e2018-80628-7

THE EUROPEAN PHYSICAL JOURNAL D

Regular Article

Associative detachment in Li+H$^-$ collisions*

Martin Čížek, Jan Dvořák, and Karel Houfek[a]

Institute of Theoretical Physics, Faculty of Mathematics and Physics, Charles University, Prague, V Holešovičkách 2, 180 00 Prague, Czech Republic

Received 1 October 2017 / Received in final form 31 January 2018
Published online 20 April 2018 – © EDP Sciences, Società Italiana di Fisica, Springer-Verlag 2018

Abstract. The cross sections and reaction rates for the associative detachment reaction $\mathrm{Li} + \mathrm{H}^- \rightarrow \mathrm{LiH} + \mathrm{e}^-$ are calculated for energies from 1 meV to 1 eV within the nonlocal discrete-state-in-continuum model. The nonlocal model yields stable results for this nonadiabatic process although there is no obvious curve crossing of the ground anion state into the continuum in adiabatic approximation.

1 Introduction

Lithium hydride molecular anion attracted a lot of attention as a smallest stable molecular anion (see [1] and references therein). The calculation of its properties is challenging due to a strong electron correlation and the nonadiabatic couplings [2]. It is also a system of large interest in astrophysics. Lithium atoms are observed in stellar atmospheres and presence of atomic hydrogen anions in stars indicates that lithium anions will be present too. Even more interesting is a possible role of molecular lithium in the chemistry of the early Universe [3,4]. Although less abundant than molecular hydrogen, neutral lithium hydride can be important cooler in formation of the first stars due to its large state density and dipole moment. The process of associative detachment (AD)

$$\mathrm{Li} + \mathrm{H}^- \rightarrow (\mathrm{LiH})^- \rightarrow \mathrm{LiH} + \mathrm{e}^-$$

can be an important source of LiH molecules, but there are neither experimental nor theoretical data for the cross sections or reaction rates available and only estimates are used in simulations [5,6].

The development of the theoretical treatment of the AD reaction

$$A + B^- \rightarrow AB + \mathrm{e}^-$$

dates back to pioneering works of Chen [7] and Herzenberg [8] in 1967. The basic assumption of most of theoretical models is that the discrete electronic state corresponding to $A + B^-$ asymptote disappears in the electron continuum describing $AB + \mathrm{e}^-$ system. The adiabatic bound discrete state thus does not exist for small separations of A and B^-, but the existence of the diabatic representation is postulated for all internuclear separations R. The detailed theoretical analysis [9] results in the effective potential for partial waves representing the nonadiabatic coupling of the discrete state with the electronic continuum, which is often approximated with the local complex potential.

This kind of treatment has been used for calculation of the associative detachment production of the hydrogen molecule since late 1960's (see for example [7,10,11]). In 1980 Bieniek [12] pointed out that the nonlocal nature of the effective interaction is essential for proper prediction of the final state distribution of the emerging H_2 molecule. Availability of accurate potential energy curves [13] and electron-H_2 scattering data [14] made finally possible accurate calculation of the AD cross sections and reaction rates [15] that proved to be in very good agreement with experimental data for both H_2 [16,17] and D_2 molecules [18].

The AD process has also been treated theoretically for collisions of negative halogen ions X^- with atomic hydrogen H [19,20]. Because these molecules possess large dipole moments the nonlocal effects proved to be even more important [21–23]. The cross sections for these systems exhibit pronounced Wigner cusps which were discovered before for the reverse process of dissociative attachment (see [24] for the first experimental evidence or [25] for a review of results for hydrogen halides).

The potential energy curves for all of the above mentioned systems have a common feature. The potential of electronic bound state corresponding to $A + B^-$ channel directly crosses to electronic continuum. The bound state disappears and is transformed into a virtual state or a resonance at small internuclear separations. The associative detachment can thus naturally be understood as a curve-crossing process. On the contrary, the ground state

* Contribution to the Topical Issue "Low Energy Positron and Electron Interactions", edited by James Sullivan, Ron White, Michael Bromley, Ilya Fabrikant and David Cassidy.

[a] e-mail: Karel.Houfek@mff.cuni.cz

of LiH^- anion is bound for all internuclear separations of Li and H^-. The purpose of this paper is to show that the nonlocal discrete-state-in-continuum model still provides accurate and stable description of the AD process.

The paper is organized as follows. In Section 2, we describe the fixed-nuclei electron structure and scattering calculations necessary to construct the nonlocal model and we also give the details of the model functions. Section 3 provides details of numerical calculation of the nuclear dynamics and gives discussion of the resulting cross sections and reaction rates. We conclude with remarks on further extensions of the model in Section 4.

2 Construction of the model

The first step in the construction of the nonlocal model for the nuclear dynamics of the LiH^- ion is a set of fixed-nuclei calculations. This involves the calculation of potential energy curves for the ground state of both the neutral LiH molecule and the LiH^- ion. The second important ingredient is the calculation of fixed-nuclei elastic scattering eigenphase sums for $e^- + LiH$ collisions. In this section we first describe these two sets of calculations and then the procedure of construction of the nonlocal model compatible with these data is briefly outlined.

2.1 Calculation of ground state potentials for LiH and LiH^-

To obtain the potential energy curves of the $X\,^1\Sigma^+$ state of LiH and the $X\,^2\Sigma^+$ state of LiH^- we used the multiconfigurational self-consistent field (MCSCF) method [26,27] followed by the multireference configuration interaction method [28] with the aug-cc-pVQZ basis of Gaussian orbitals developed by Dunning [29]. The complete active space in MCSCF calculations consisted of ten active orbitals with four or five active electrons for LiH and LiH^- respectively. All calculations were performed using the MOLPRO package [30,31]. The data for the potential energy curves were thus obtained on the interval of internuclear distances $R \in \langle 1.5, 40\rangle$ with irregular spacing 0.1–1.0 bohr. The data were interpolated by cubic splines within this interval. For internuclear distances smaller then 1.5 bohr we extrapolated using a Morse potential fitted from the data on the interval 1.5–2.0 bohr. For distances larger than 40 bohr, we used for extrapolation the known polarizability of lithium atom $\alpha = 164.1$ a.u., i.e. $V_{\rm ion}(R) = -0.5\alpha R^{-4}$.

The potential energy curves obtained in this work are close the ones of Gadéa and Leininger [2] and of Chang et al. [32], the latter we used for comparison in Figure 1. The accuracy of the data can be estimated from the calculated electron affinities. We obtained the values of 620 meV and 740 meV within the present quantum chemistry description for Li and H atoms respectively, which correspond well with the experimental values of 618 meV and 754 meV [33]. Since the molecular anion is electronically bound for all internuclear separations we can also calculate the electron affinity for the LiH molecule (taking into account the lowest vibrational level in both potentials). We thus obtained the value of 320 meV which is by 22 meV lower than the experimental value of 342 meV [33] and by 10–12 meV lower than previous theoretical results [2,32]. Although the electron affinities correspond rather well to values in the literature, the dissociation energies for both LiH and LiH^- are less accurate as we can clearly see from comparison with the data of Chang et al. [32] in Figure 1. Thus we expect that relative positions and shapes of our potential energy curves are accurate within 50–70 meV.

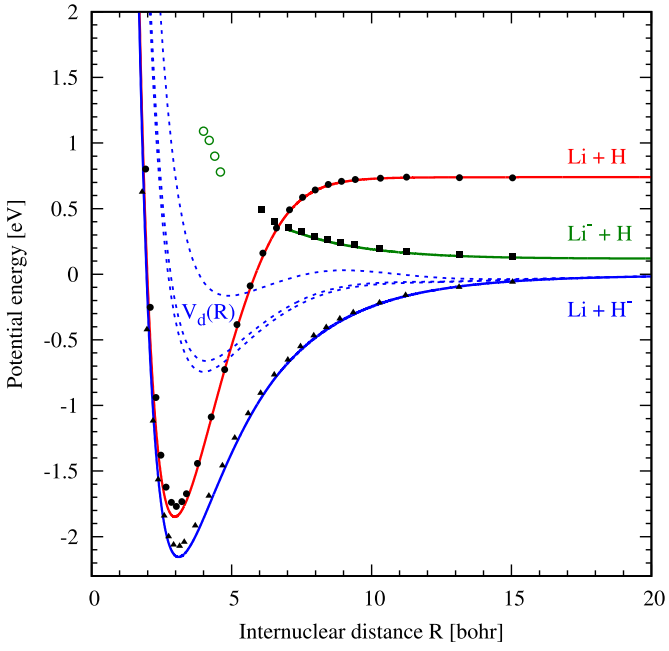

Fig. 1. Potential energy curves (solid lines) for neutral and anionic LiH system compared with data of Chang et al. [32] (points). Positions of the resonances seen in Figure 2 are indicated as circles. The dashed lines show the discrete state potential for models 1, 2, 3 (from top to bottom).

In Figure 1 we can see that the ground state of the anion (solid blue line) is located below the ground state of the neutral molecule (solid red line) for all R. Nevertheless, the two curves come very close to each other for short internuclear distances and we expect strong coupling of the anion state with the electron scattering continuum. For completeness we also show the excited anion state (green line) connected to the Li^-+H asymptote which is not used in this work. Later in this section we will discuss the construction of the diabatic representation of the anion ground state which determines the potential $V_d(R)$. Three possible choices are shown as dotted blue line (see the Sect. 2.3).

2.2 Scattering eigenphase sums for e^-+LiH

The fixed-nuclei eigenphase sums for the electron scattered from the LiH molecule in its ground state were calculated using the R-matrix method [34] as implemented in the UK molecular R-matrix suite of codes [35,36]. The target molecule was described on the MCSCF level, or

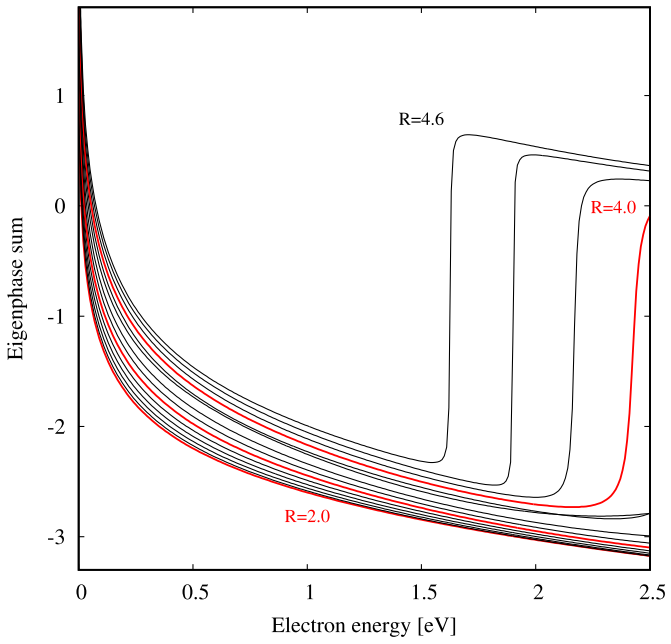

Fig. 2. Fixed-nuclei eigenphase sums for e^-+LiH scattering at internuclear separation 2.0, 2.2,..., 4.6 bohr (from bottom to top).

to be more specific, the complete active space with 4 electrons in 8 active molecular orbitals was used. The target was described using the cc-pVTZ basis of Gaussian orbitals, but the two most diffuse s and p Gaussian basis functions were changed to be less diffuse to avoid problems with the linear dependence between target basis functions and the functions used to expand the continuum orbitals. The close-coupling model [34] with 1 target state and 10 virtual orbitals was used as model for scattering within the R-matrix approach. This choice was validated by comparing the potential energy curves with the results of the MOLPRO calculation from the previous section.

The energy-dependent eigenphase sums for 14 internuclear distances R =2.0, 2.2,..., 4.6 are shown in Figure 2. The eigenphase sums should diverge logarithmically at zero energy [37,38], but this divergence is hidden in the energy resolution of the figure. Resonances visible in the eigenphase sums for $R > 1.5$ are unrelated to the potential energy curve for Li+H^-. Their positions (green circles in Fig. 1) indicate that the resonances are continuation of the Li^-+H curve into the region where the bound excited electronic state of the anion transforms into the metastable resonance state. Similar resonances were found also in R-matrix calculation of Antony et al. [39].

2.3 Construction of the nonlocal model for nuclear dynamics of Li+H^- system

The present procedure for the construction of the nonlocal model from fixed-nuclei data described above follows to a large degree the procedure proposed in [40] for the H+Br^- system. The scattering eigenphase sums are decomposed into a resonance and a background part $\delta = \delta_{\rm bg} + \delta_{\rm res}$. The dependence of the background part on both electron energy ϵ and internuclear distance R is assumed to be smooth and we fit it with a linear function

$$\delta_{\rm bg}(\epsilon, R) = A\epsilon + BR + C. \quad (1)$$

The resonance part is described by projection-operator formalism in the model of a discrete state in the continuum (see for example the review article [41]) with the generalized Breit-Wigner formula

$$\delta_{\rm res} = -\arctan\left(\frac{\Gamma(\epsilon, R)/2}{\epsilon - V_d(R) + V_0(R) - \Delta(\epsilon, R)}\right). \quad (2)$$

The function $V_0(R)$ is the known potential energy of the ground state of the neutral LiH molecule. The width function $\Gamma(\epsilon, R)$ is assumed to be of the form

$$\Gamma(\epsilon, R) = a(R)\left(\frac{\epsilon}{b(R)}\right)^{\alpha} {\rm e}^{-\epsilon/b(R)}, \quad (3)$$

which makes possible analytic evaluation of the level-shift function

$$\Delta(\epsilon, R) = \frac{1}{2\pi}{\rm p.v.}\int \frac{\Gamma(\epsilon', R)}{\epsilon - \epsilon'}{\rm d}\epsilon'. \quad (4)$$

Furthermore, the discrete state potential function $V_d(R)$ is constrained by the position of the ground state potential $V_{\rm ion}(R)$ since the relation between the diabatic discrete state and the adiabatic ion potential within the discrete-state-in-continuum model reads [19,40]

$$V_d(R) + \Delta(\epsilon, R)|_{\epsilon = V_{\rm ion}(R) - V_0(R)} = V_{\rm ion}(R). \quad (5)$$

Given the fixed-nuclei data for $V_0(R)$, $V_{\rm ion}(R)$ and phase-shifts $\delta(\epsilon, R)$ we can try to find the constants A, B, C and α and the smooth functions $a(R)$ and $b(R)$ so that the formulae (1)–(5) reproduce these data as accurately as possible. The resulting fit is neither perfect nor unique. This is not surprising since the choice of the discrete state within the model is to a large degree arbitrary [42]. Different fits can for example lead to different splitting of the anion potential into the discrete-state potential and the level shift in the formula (5). To check the sensitivity of the final cross sections and reaction rates to this ambiguity we constructed three different models numbered as model 1, 2 and 3. The discrete-state potential $V_d(R)$ for these three models is shown in Figure 1 with dashed lines. The eigenphases calculated from (1)–(4) follow the data in Figure 2 for all R and energy ϵ = 0.05–1.5 eV within 0.2 rad. This is not a perfect fit but we will see in the next section that the resulting cross sections and reaction rates are quite insensitive to the specific choice of the model.

3 Cross sections and reaction rates

In this section we first describe briefly the theory of anion-atom scattering within the nonlocal model including the details of numerical treatment of the resulting equations.

The behavior of calculated cross sections and rates is discussed in the second part.

3.1 Details of the nonlocal calculation of the reaction dynamics

The method for the treatment of the AD process has been described in detail previously in [15] or in the review [43] and is based on projection-operator treatment of vibrational dynamics in electron-molecule collisions within the discrete-state-in-continuum model (see [41,43] for review). We give only short account of basic equations needed for description of the numerical details specific for these calculations. The basic equation is the Lippmann-Schwinger equation for the lth partial wave expansion coefficient of the full wave function projected on the discrete state

$$|\psi_l\rangle = |\phi_l\rangle + G_l(E)F_l(E)|\psi_l\rangle, \tag{6}$$

where $|\phi_l\rangle$ is the partial wave for the potential scattering in the discrete-state potential V_d, $G_l(E)$ is the retarded Green's function in this potential and $F_l(E)$ is the nonlocal energy-dependent potential due to coupling of the discrete state to the electronic scattering continuum and it can be expanded in the vibrational states $|\chi_n\rangle$ of the neutral molecule

$$\left[T_N + V_0(R) + \frac{l(l+1)}{2\mu R^2}\right]|\chi_n\rangle = E_n|\chi_n\rangle, \tag{7}$$

where T_N is the kinetic-energy operator for the nuclei and $\mu \doteq 1606.5$ a.u. is the reduced mass of the LiH system. Using these functions the effective potential reads

$$\langle R|F_l(E)|R'\rangle = \sum_n \chi_n(R)\left[\tilde{\Delta}(\epsilon_n,R,R') - \frac{i}{2}\tilde{\Gamma}(\epsilon_n,R,R')\right]\chi_n(R'),$$

where $\epsilon_n = E - E_n$ and

$$\tilde{\Gamma}(\epsilon,R,R') = \sqrt{\Gamma(\epsilon,R)\Gamma(\epsilon,R')},$$
$$\tilde{\Delta}(\epsilon,R,R') = \frac{1}{2\pi}\text{p.v.}\int \frac{\tilde{\Gamma}(\epsilon',R,R')}{\epsilon-\epsilon'}\mathrm{d}\epsilon'. \tag{8}$$

The vibrational wavefunctions $|\chi_n\rangle$ are found using the DVR method with the Fourier basis. The resulting functions are calculated on the regular grid of 6000 points on the interval $R \in \langle 0, 20\rangle$ a.u. For the representation of the nonlocal potential $F_l(E)$ on this grid we use the first 90 functions $|\chi_n\rangle$ including functions from the discretised dissociation continuum. The solution ϕ_l of the scattering problem for the local potential V_d and the Green's function $G_l(E)$ are found on a more extended grid (depending on energy typically R goes up to 150 bohr). The equation (6) with the potential (8) is solved using the iterative Schwinger-Lanczos algorithm [44]. The cross section is finally calculated from the formula

$$\sigma_{\text{AD}} = \frac{2\mu}{K^3}\sum_{ln}(2l+1)|\langle\chi_n|\sqrt{\Gamma(E-E_n)}|\psi_l\rangle|^2. \tag{9}$$

For more numerical details see [45,46].

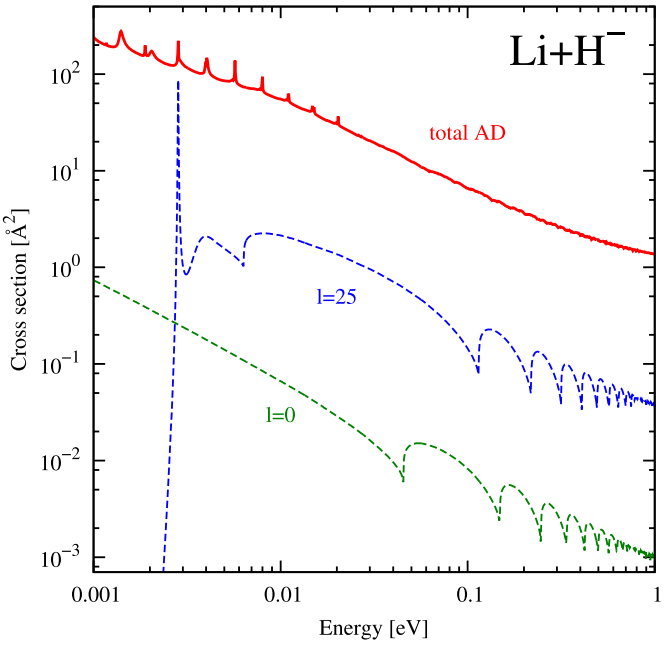

Fig. 3. The integral cross section for associative detachment in Li+H$^-$ collision. Examples of contribution of the individual partial waves are also shown for the orbital angular momenta $l = 0$ and $l = 25$ with dashed lines.

3.2 Discussion of the results

The resulting cross section for the AD process is shown in Figure 3. The total cross section (solid line) is an overall monotonously decreasing function with structures of sharp peaks and cusps superimposed on it. The overall decreasing shape is a consequence of the attractive character of the Li+H$^-$ potential. The origin of the structures is best understood if we look at individual partial-wave components of the cross section (dashed lines in Fig. 3). The partial wave component for $l = 0$ exhibits cusps for energies $E > 0.04$ eV. These cusps are Wigner cusps due to contributions of the individual vibrational states (7). These structures are also seen in the total cross section, but since the total cross section is a sum of 60 individual partial waves the structures almost disappear in the logarithmic plot. Similar structures are present also in the AD cross sections for halogen anions [20]. The sharp peaks for $E < 0.03$ eV originate in higher partial waves. We can nicely see it on the $l = 25$ contribution in Figure 3. These peaks come from orbiting resonances similar to those in the H + H$^-$ system [47] and in hydrogen halides [48].

In the previous section we constructed three different nonlocal models with discrete-state potentials differing by as much as 0.5 eV. This difference is partially compensated with the level shift function Δ present in the nonlocal

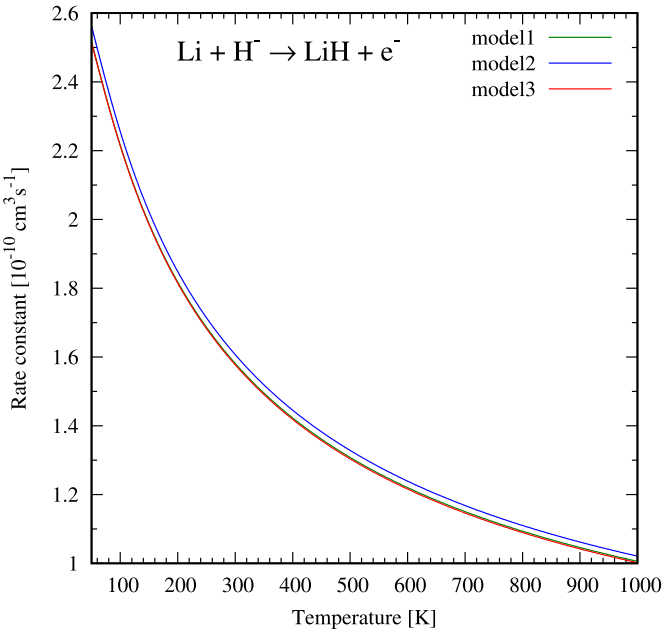

Fig. 4. The associative detachment reaction rates and their sensitivity to the choice of model parameters.

potential (8) but the size of the nonlocal coupling is quite different among the three models. The cross sections for all three models differ by at most 2% in the studied energy range. The difference that would be indistinguishable in the logarithmic scale in Figure 3. This is very important observation validating our approach in two respects. First, it shows that the ambiguity of the fitting procedure does not have significant influence on the final cross sections. Second, we could doubt whether the whole idea of using the nonlocal discrete-state-in-continuum model is right for a system without obvious curve crossing. But the stability of the cross sections with respect to model details ensures us that this way of description of the nonadiabatic coupling between the discrete state of the anion molecule and the electron scattering continuum is correct.

We also calculated the AD reaction rates by averaging the product of velocity and the cross section over the Maxwell-Boltzmann distribution of velocities [20]. The results are shown in Figure 4. Here we show explicitly the results for all three models. The difference is again within 2%, but now we can distinguish it since linear scale is used.

Note that the resulting reaction rates can be fitted with the formula

$$\log_{10} k_{\mathrm{AD}} = a(\log_{10} t)^2 + b \log_{10} t + c$$

within the same accuracy (<2%) as the difference among the individual models. The numerical values of parameters are $a = -0.0996, b = 0.15, c = -9.56$ for temperatures in Kelvin and rates in cm^3/s.

4 Conclusions and future prospects

We have calculated the reaction rate for the associative detachment process $\mathrm{Li} + \mathrm{H}^- \rightarrow \mathrm{LiH} + \mathrm{e}^-$ within the nonlocal model which can be used in simulations of chemistry of the early Universe or stellar atmospheres. The calculated reaction rate is a decreasing function of temperature. The maximum value at temperature 100 K is more than one order of magnitude smaller than the Langevin rate and almost two times smaller than the estimated value of $4 \times 10^{-10}\,\mathrm{cm}^3\mathrm{s}^{-1}$ used in the simulations [5] (note that a rate independent of temperature was used in the simulations). We should note that recent calculations [49] of the charge transfer cross sections also give estimates of detachment rates, but these are for higher energies (temperatures) than are considered in our work and include only collisional detachment, but not formation of the neutral molecule because the coupling to the electron continuum at short internuclear distances is not included in their calculation. Because our results show that the associative detachment rate is several orders of magnitude larger than results of [49] at temperature 1000 K we can conclude that to estimate detachment rates at low temperatures one must take into account the associative detachment process.

In future we also want to include the second associative detachment channel $\mathrm{Li}^- + \mathrm{H} \rightarrow \mathrm{LiH} + \mathrm{e}^-$. To achieve this goal we have to extend the fixed-nuclei electron-scattering calculations into the region of internuclear distances $R \in \langle 5, 7 \rangle$ bohr near the crossing of the potentials of the excited anion state with the ground state of the neutral LiH molecule. Currently we obtained unstable results in this region using the R-matrix method. After resolving these problems we will construct a model including both anion states which can also be used for calculation of low-energy inelastic electron collisions with LiH molecules, electron photodetachment from the ground state of the LiH^- ion and charge transfer in $\mathrm{Li} + \mathrm{H}^-$ and $\mathrm{Li}^- + \mathrm{H}$ collisions.

The work is supported by the Charles University, project GAUK No. 643216, and by the Grant Agency of Czech Republic under contract number GACR 16-17230S.

Author contribution statement

K. Houfek performed quantum chemical and scattering calculations to provide fixed-nuclei data. J. Dvořák used these data to construct the nonlocal model for nuclear dynamics and calculated the cross sections and reaction rates under supervision of M. Čížek. All authors contributed to data interpretation, manuscript preparation and discussion of the results.

References

1. S. Nasiri, M. Zahedi, Comput. Theor. Chem. **1114**, 106 (2017)
2. F.X. Gadéa, T. Leininger, Theor. Chem. Acc. **116**, 566 (2006)
3. S. Lepp, P.C. Stancil, A. Dalgarno, J. Phys. B **35**, R57 (2002)
4. S.C.O. Glover, J. Chluba, S.R. Furlanetto, J.R. Pritchard, D.W. Savin, Adv. At. Mol. Opt. Phys. **63**, 135 (2014)

5. P.C. Stancil, S. Lepp, A. Dalgarno, Astrophys. J. **458**, 401 (1996)
6. S. Bovino, M. Tacconi, F.A. Gianturco, D. Galli, F. Palla, Astrophys. J. **731**, 107 (2011)
7. J.C.Y. Chen, Phys. Rev. **156**, 12 (1967)
8. A. Herzenberg, Phys. Rev. **160**, 80 (1967)
9. R.J. Bieniek, Phys. Rev. A **18**, 392 (1978)
10. J.C.Y. Chen, J.L. Peacher, Phys. Rev. **168**, 56 (1968)
11. R.J. Bieniek, A. Dalgarno, Astrophys. J. **228**, 635 (1979)
12. R.J. Bieniek, J. Phys. B **13**, 4405 (1980)
13. J. Senekowitsch, P. Rosmus, W. Domcke, H.-J. Werner, Chem. Phys. Lett. **111**, 211 (1984)
14. M. Berman, M. Mündel, W. Domcke, Phys. Rev. A **31**, 641 (1985)
15. M. Čížek, J. Horáček, W. Domcke, J. Phys. B **31**, 2571 (1998)
16. H. Kreckel, H. Bruhns, M. Čížek, S.C.O. Glover, K.A. Miller, X. Urbain, D.W. Savin, Science **329**, 69 (2010)
17. K.A. Miller, H. Bruhns, J. Eliášek, M. Čížek, H. Kreckel, X. Urbain, D.W. Savin, Phys. Rev. A **84**, 052709 (2011)
18. K.A. Miller, H. Bruhns, M. Čížek, J. Eliášek, R. Cabrera-Trujillo, H. Kreckel, A.P. O'Connor, X. Urbain, D.W. Savin, Phys. Rev. A **86**, 032714 (2012)
19. M. Čížek, J. Horáček, W. Domcke, Phys. Rev. A **60**, 2873 (1999)
20. K. Houfek, M. Čížek, J. Horáček, W. Domcke, Phys. Rev. A **66**, 062702 (2002)
21. M. Čížek, J. Horáček, F.A.U. Thiel, H. Hotop, J. Phys. B **34**, 983 (2001)
22. S. Živanov, M. Allan, M. Čížek, J. Horáček, F.A.U. Thiel, H. Hotop, Phys. Rev. Lett. **89**, 073201 (2002)
23. S. Živanov, M. Čížek, J. Horáček, M. Allan, J. Phys. B **36**, 3513 (2003)
24. K. Rohr, F. Linder, J. Phys. B **8**, L200 (1975)
25. M. Čížek, J. Horáček, M. Allan, W. Domcke, Czech. J. Phys. **52**, 1057 (2002)
26. P.J. Knowles, H.-J. Werner, Theor. Chim. Acta **84**, 95 (1992)
27. H.-J. Werner, P.J. Knowles, J. Chem. Phys. **82**, 5053 (1985)
28. P.J. Knowles, H.-J. Werner, Chem. Phys. Lett. **115**, 259 (1985)
29. T.H. Dunning Jr., J. Chem. Phys. **90**, 1007 (1989)
30. H.-J. Werner, P.J. Knowles, G. Knizia, F.R. Manby, M. Schütz, WIREs Comput. Mol. Sci. **2**, 242 (2012)
31. H.-J. Werner et al., MOLPRO, version 2012.1, a package of ab initio programs, see http://www.molpro.net
32. D.T. Chang, K. Reimann, G. Surratt, G.I. Gellene, P. Lin, R.R. Lucchese, J. Chem. Phys. **117**, 5757 (2002)
33. J.C. Rienstra-Kiracofe, G.S. Tschumper, H.F. Schaefer, S. Nandi, G.B. Ellison, Chem. Rev. **102**, 231 (2002)
34. J. Tennyson, Phys. Rep. **491**, 29 (2010)
35. L.A. Morgan, J. Tennyson, C.J. Gillan, Comput. Phys. Commun. **114**, 120 (1998)
36. J.M. Carr, P.G. Galiatsatos, J.D. Gorfinkiel, A.G. Harvey, M.A. Lysaght, D. Madden, Z. Mašín, M. Plummer, J. Tennyson, H.N. Varambhia, Eur. Phys. J. D **66**, 58 (2012)
37. H. Friedrich, *Scattering theory* (Springer, Berlin, 2013)
38. I.I. Fabrikant, J. Phys. B **49**, 1 (2016)
39. B.K. Antony, K.N. Joshipura, N.J. Mason, J. Tennyson, J. Phys. B **37**, 1689 (2004)
40. M. Čížek, J. Horáček, A.-Ch. Sergenton, D.B. Ppović, M. Allan, W. Domcke, T. Leininger, F.X. Gadea, Phys. Rev. A **63**, 062710 (2001)
41. W. Domcke, Phys. Rep. **208**, 97 (1991)
42. K. Houfek, T.N. Rescigno, C.W. McCurdy, Phys. Rev. A **77**, 012710 (2008)
43. P. Čárský, R. Čurík (eds.), *Low-energy electron scattering from molecules, biomolecules and surfaces* (CRC Press, Boca Raton, 2012)
44. H.-D. Meyer, J. Horáček, L.S. Cederbaum, Phys. Rev. A **43**, 3587 (1991)
45. M. Čížek, Resonant processes in atomic collisions: theoretical considerations and calculations, Ph.D. thesis, Charles University, Prague, 1999
46. J. Dvořák, Associative electron detachment in collision of negative ion, Master thesis, Charles University, Prague, 2017
47. M. Čížek, J. Horáček, W. Domcke, Phys. Rev. A **75**, 012507 (2007)
48. M. Čížek, J. Horáček, Int. J. Mass Spectrom. **280**, 149 (2009)
49. Y. Wu, X.H. Lin, B. Yan, G.J. Wang, R.K. Janev, J. Phys. B **49**, 035203 (2016)